Vol. 18, pp. 244–253 (2021)
doi: 10.2142/biophysico.bppb-v18.027

Biophysics and Physicobiology
https://www.jstage.jst.go.jp/browse/biophysico/

Review Article (Invited)

Application of quantitative cell imaging using label-free optical diffraction tomography

Chan-Gi Pack [1,2]

[1] *Convergence Medicine Research Center (CREDIT), Asan Institute for Life Sciences, Asan Medical Center, Seoul 05505, Republic of Korea*
[2] *Department of Convergence Medicine, University of Ulsan College of Medicine, Seoul 05505, Republic of Korea*

Received July 1, 2021; Accepted October 11, 2021;
Released online in J-STAGE as advance publication October 15, 2021
Edited by Haruki Nakamura

The cell is three-dimensionally and dynamically organized into cellular compartments, including the endoplasmic reticulum, mitochondria, vesicles, and nucleus, which have high relative molecular density. The structure and functions of these compartments and organelles may be deduced from the diffusion and interaction of related biomolecules. Among these cellular components, various protein molecules can freely access the nucleolus or mitotic chromosome through Brownian diffusion, even though they have a densely packed structure. However, physicochemical properties of the nucleolus and chromosomes, such as molecular density and volume, are not yet fully understood under changing cellular conditions. Many studies have been conducted based on high-resolution imaging and analysis techniques using fluorescence. However, there are limitations in imaging only fluorescently labeled molecules, and cytotoxicity occurs during three-dimensional imaging. Alternatively, the recently developed label-free three-dimensional optical diffraction tomography (ODT) imaging technique can divide various organelles in cells into volumes and analyze them by refractive index, although specific molecules cannot be observed. A previous study established an analytical method that provides comprehensive insights into the physical properties of the nucleolus and mitotic chromosome by utilizing the advantages of ODT and fluorescence techniques, such as fluorescence correlation spectroscopy and confocal laser scanning microscopy. This review article summarizes a recent study and discusses the future aspects of the ODT for cellular compartments.

Key words: label-free 3D imaging, intracellular microenvironment, molecular crowding, diffusion coefficient

Significance

The cell is three-dimensionally and dynamically organized into cellular compartments, including the endoplasmic reticulum, mitochondria, nucleus, and chromosome, which have high relative molecular density. Many previous studies have analyzed these dynamic characteristics by relying only on fluorescence microscopy and specific biomarkers. However, physicochemical properties of the nucleolus and chromosomes, such as molecular density and microenvironment, are not yet fully understood under changing cellular conditions. In addition to the observation of fluorescent biomarkers, ODT will be of great help in comprehensively understanding changes in the highly crowded microenvironment of each organelle in the cell.

Introduction

Fluorescence imaging techniques such as confocal laser scanning microscopy (CLSM) can determine the intracellular spatial distribution of a target molecule by detecting a fluorescent probe bound to that molecule. In addition, when using

Corresponding author: Chan-Gi Pack, Asan Institute for Life Sciences, Asan Medical Center, Seoul 05505, Republic of Korea. ORCID iD: https://orcid.org/0000-0002-6578-3099, e-mail: changipack@amc.seoul.kr

living cells, information involving the temporal dynamics of the target molecule can be obtained quantitatively with high accuracy. Therefore, CLSM is an indispensable method for research in cell biology and basic medicine. Furthermore, fluorescence correlation spectroscopy (FCS) can quantitatively analyze information on the diffusional motion and interaction of fluorescent molecules in living cells and aqueous solutions. Recently, FCS has also been incorporated into CLSM to be used in combination with fluorescence imaging [1-6].

On the other hand, the conventional phase-contrast microscope developed by Frits Zernike allows the observation of transparent cells without staining [7]. This technique visualizes phase shifts of light by transforming phase shift gradients into intensity variations. This phase shift is realized by adding a phase filter to a general optical microscope and using the interference phenomenon of light. However, the intensity variations are mixed with other intensity variations, making it difficult to extract quantitative information. The limitation has been remedied by quantitative phase imaging (QPI) using holographic technology. In the conventional two-dimensional (2D) digital holography technology, the phase delay information is obtained by measuring the laser interference pattern [8,9]. Therefore, this made it possible to measure the contour (image) and the thickness. Moreover, by adopting three-dimensional (3D) holography technology, such as QPI, it has become possible to obtain quantitative information such as sample volume, refractive index (RI), and thickness, even for non-uniform samples. Currently, QPI is becoming an effective biophysical method for simultaneously examining 3D images and RI values of cells.

The RI value is closely related to fluidic viscosity in aqueous solutions. FCS is a method for determining the diffusion coefficient (D) of a fluorescent probe and investigating fluidic viscosity and molecular crowding in solutions and cells [10,11]. Additionally, the diffusional motion of the probe changes depending on the size, density distribution, and movement of the polymer surrounding the probe. It is also possible to predict the molecular crowding state in the solution from the D value of the probe using a uniform solution with known conditions. However, observing the diffusional motion of the probe is not enough to understand the heterogeneous crowding state consisting of biomolecules and complexes of various unknown sizes, such as in cells. To understand the cellular crowding state, it would be advantageous to compare together the spatial distribution of refractive indices for various structures (i.e., organelle and compartment) distributed in cells and D values. Therefore, it was considered practical to link the QPI method to the conventional confocal fluorescence microscope and FCS to understand the state of molecular crowding in living cells more accurately.

Molecular Density and Fluidic Property of Cellular Compartments

Although cells contain substantial water, biomolecules of various sizes, such as DNA/RNA, lipids, and proteins, are locally and heterogeneously distributed at high density inside each organelle or compartment. The average intracellular concentrations of proteins and nucleic acids are approximately 50–250 g/L and 20–50 g/L, respectively, depending on the mammalian cell type [12,13]. Biomolecules, proteins in particular, move to each cell organelle or compartment and interact with target molecules to function according to physiological conditions. However, in such a high-density environment, biochemical reactions may be activated, or molecular crowding may change the diffusional motion of molecules in a size-dependent manner [12,14-19]. It is still unclear to what extent this phenomenon occurs in the cell or which molecule exerts its function through this effect. Therefore, it is first necessary to quantitatively evaluate the molecular density or the characteristics of the local microenvironment inside living cells. In this respect, the FCS method, which measures the concentration (c) and D value of a fluorescent probe molecule present in a solution or living cell, has been used to evaluate the microenvironment inside each cell compartment or to measure the diffusional behavior of a specific molecule [6,20,21]. Previous studies analyzing cells expressing multimeric green fluorescent protein (GFP) probes of different sizes [10,11] found that proteins up to 150 kD can freely diffuse within the cell, and the fluidic viscosity of the cytoplasm and nucleoplasm is about 3 to 4 times higher than that of water. Moreover, it was suggested that the GFP probes could freely access the nucleolus, and its viscosity is about 10 to 18 times higher than that of water. Interestingly, it was also demonstrated that diffusion inside the nucleolus is highly dependent on the size of the GFP probe and sensitive to physiological stress, such as transcription inhibition by actinomycin D [11]. Although the diffusional motion of various probes provides information regarding the change of the microenvironment in the cell nucleus, it is still unclear what kind of change in the surrounding macroenvironment causes the change in probe diffusion. If the density distribution for the surrounding volume, including the detection volume (~0.12 fL) measured by FCS can be defined, it will be possible to establish the relationship more accurately between the probe and the environmental change surrounding it.

The RI value of the sample solution is proportional to the molecular density contained in the sample due to the relationship of $n = n_0 + \alpha c$ [22], where n and n_0 indicate the RI values of the sample and the surrounding medium, respectively, and α and c indicate the refractive index increment and the concentration of biomolecules, respectively. Therefore, if the RI value is determined from the QPI measurement, the molecular density of biomolecules contained in the sample can be estimated. The RI increment α depends on the sample type, light source wavelength, and temperature; however, many proteins have the same α value, and when using a light source of 532 nm, α is constant (0.2 mL/g) [22]. Solution samples of DNA and nucleosomes have α values ranging from 0.15 to 0.18 mL/g, which are smaller than that of

proteins [23]. In actual QPI measurements, the difference in RI can be detected up to 0.0001, and the change in protein concentration can be detected up to about 0.5 mg/mL. The RI representing the molecular density in a homogenous solution is proportional to the viscosity of the solution. Viscosity is inversely proportional to the diffusion coefficient when the temperature and the size of the probe molecule are constant, according to the Stokes-Einstein relation [6,10]; thus, the relationship between the average RI of a solution sample and the diffusion coefficient of a specific probe present can be determined experimentally. Figure 1 shows the relationship between the RI and *D* values obtained by measuring the RI of solutions with a known sucrose concentration (Fig. 1a) and the *D* value of the rhodamine 6G probe included in the same solutions (Fig. 1b). Similarly, if solutions containing various solutes and a fluorescent probe are used, more detailed relationships between RI and *D* values can be established experimentally. As shown in Figure 1, the RI values of various homogenous solutions with well-known viscosities can be easily measured using a refractometer or other method [24]. In addition, for large heterogeneous systems, such as living cells, RI values can be obtained through QPI analysis. In the next sections, two studies analyzing the molecular density (RI value) through imaging organelles of living cells, especially the nucleolus and mitotic chromosome, using label-free QPI will be discussed.

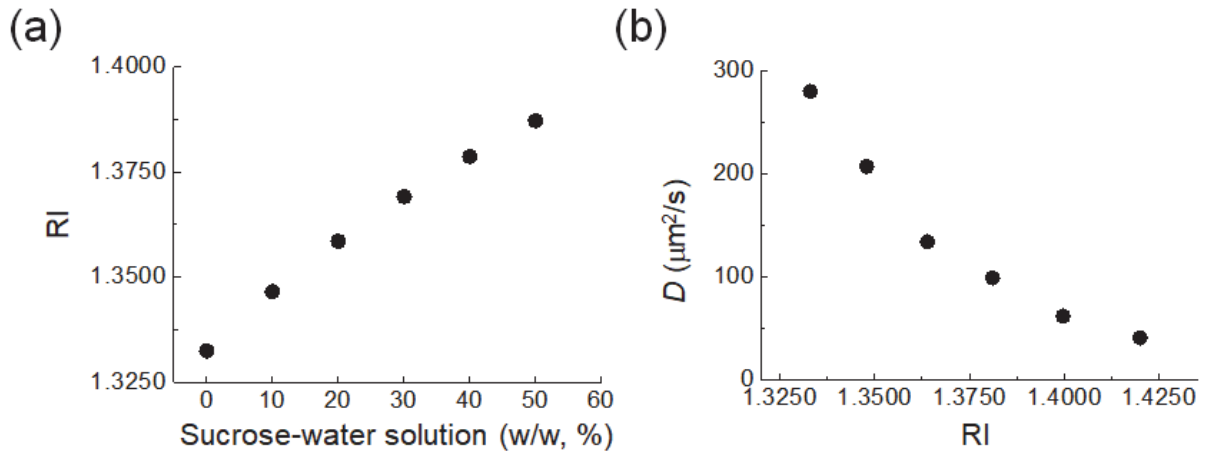

Figure 1 Experimental determination of the relationship between the diffusion coefficient (*D)* values of rhodamine 6G and the refractive index (RI) values of the aqueous medium. (a) Measured RI values of water and various sucrose–water solutions of known concentration at 25 ℃ are shown. The RI of the solution samples was measured using a refractometer. (b) The relationship between the measured RI values of the solutions obtained and measured *D* values of rhodamine 6G in water and sucrose–water solutions.

Imaging Single Living Cells and Evaluation of Physical Characteristics of the Nucleolus Using Optical Diffraction Tomography

There are various ways to realize QPI [8,25-27]. In this review, cell analysis using optical diffraction tomography (ODT), a well-established QPI technique, will be described. In ODT, a 3D holographic image is reconstructed from 2D hologram images obtained by irradiating a laser light source at various angles using a digital mirror device [28,29]. This is similar to obtaining a 3D image using X-ray computed tomography. The 3D image obtained in this way includes the volume and RI of a specific component. For detailed principles of ODT, please refer to the literature. In a previous study, Kim et al. applied ODT to live HeLa cells to demonstrate the accuracy of RI distribution images of the nucleolus among the organelles [30]. Due to the high molecular density of the nucleolus compared with other organelles, it was expected that tomographic RI images would have a clear nucleolar structure compared with other nuclear and cytosolic compartments in S-phase. Since various marker proteins capable of fluorescence imaging of the nucleolus, such as B23, are well-known, the nucleolus is suitable for 3D fluorescence imaging using CLSM. Therefore, morphological features and volume were compared using 3D nucleolus images obtained using ODT and CLSM, respectively. In addition, the possibility of non-uniform RI distribution within the nucleolus was also examined through ODT analysis adopting various RI ranges.

Figure 2 shows a representative raw 3D ODT image of a live HeLa cell (Fig. 2a) and four different RI rendered images using the same raw image (Fig. 2b-e). The raw image presents multiple large components of high molecular density (white) in the nucleus, the high-density contour of the thin nuclear membrane, and the fibric structure in the cytosol. Figure 2b presents the cell simply described by two broad RI ranges (low and high). The low RI range fills both the cytosol and nucleus, while the high RI range homogenously fills large and high-density components in the nucleus. Besides the nucleoli, discontinuous nuclear membrane and high-density components in the perinuclear region of the

cytoplasm were partially presented since their RI also falls within the high RI range. Figure 2c shows the same cell described by one narrow RI range and the same high and broad RI range presented in Figure. 2b. In contrast to Figure 2b, the narrow RI range mainly expresses the nucleoplasm and expresses some cytoplasm regions adjacent to the nuclear membrane. Figure 2d shows the rendering result of dividing the low RI region shown in Figure 2b into three RI regions. Interestingly, many areas of the nucleoplasm exhibit a slightly higher RI than that of the cytoplasm.

The nucleolus has the highest molecule density in the nucleus; thus, the large components inside the nuclear membrane were assumed to be nucleoli. For simplicity, other small components with high molecular density but less than 2 μm in diameter were not considered nucleoli as they could also be Cajal or promyelocytic leukemia (PML) nuclear bodies [31-33]. The distinction between the Cajal or PML body and the nucleolus can be analyzed separately by ODT and fluorescence imaging. The nucleolus has heterogeneous sub-compartments with different molecular densities, such as the fibrillar center, the dense fibrillary component, and the granular component; therefore, the single broad RI range shown in Figure 2b, c, d was divided into three narrow RI ranges (low, middle, and high) and pseudo-colored RI images of the nucleolus were examined for each narrow range (Fig. 2e). The low RI range homogenously fills a broad range and the outer part of the nucleolus, whereas the middle and high RI ranges occupy inner heterogeneous volumes in the nucleolus. Interestingly, the high RI ranges occupy a small volume surrounded by the region of the middle RI range. Considering the three well-known structures of the nucleolus, it would be reasonable to divide one broad RI range into multiple narrow ranges to represent the heterogeneous molecular density of the nucleolus adequately. However, it is unclear whether each volume represented by the RI values corresponds to the three structures seen in electron microscopy. Correlative or complementary analysis with fluorescent or electron microscopic methods will help uncover such details.

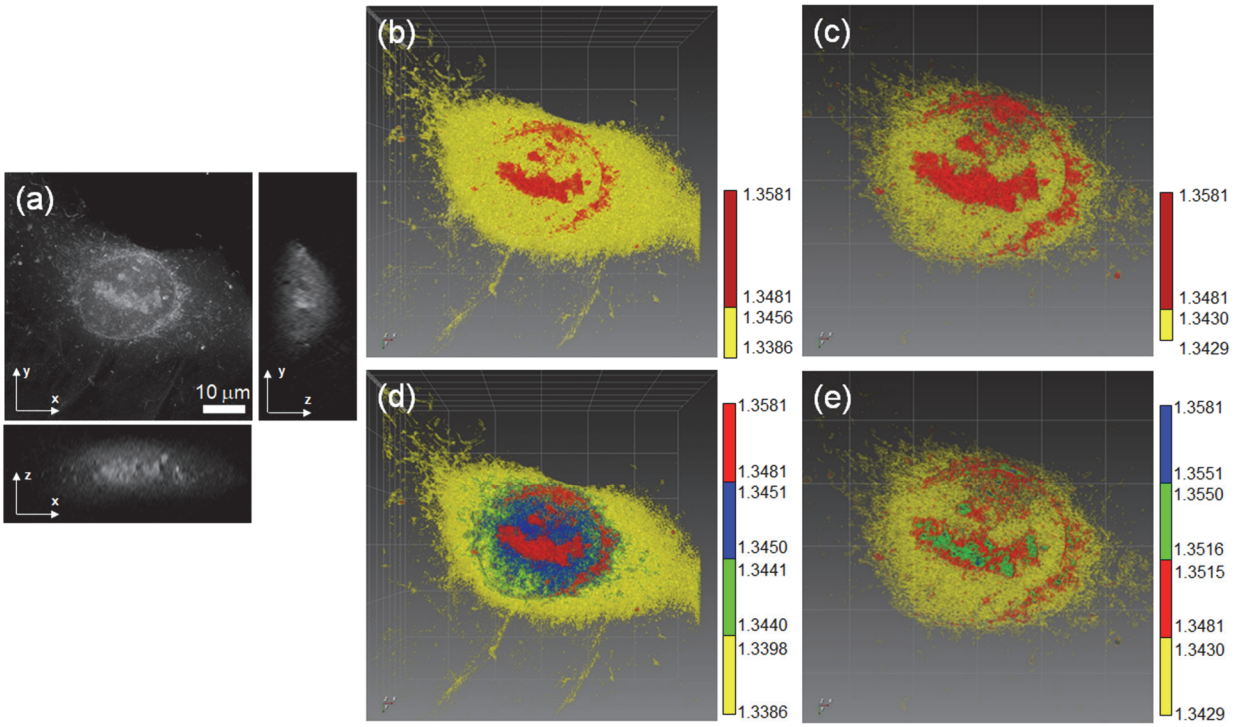

Figure 2 The nucleolus of a live HeLa cell analyzed by label-free optical diffraction tomography (ODT). (a) Raw ODT image of a HeLa cell. Cross-sectional slices of the 3D image in the x-y, x-z, and y-z planes of the cell are shown. The raw image can be rendered with various refractive index (RI) ranges as shown in b, c, d, e. (b) A pseudo-colored RI image of the cell represented by tow broad RI ranges for describing the entire cytosol (yellow) and nucleoli (red). Note that a part of nuclear membranes and the perinuclear regions of the cytosol are also expressed in the same RI region as the nucleolus. (c) A pseudo-colored RI image of the same cell. The nucleoplasm is represented by a narrow RI range (yellow) and the multiple nucleoli by a broad RI range (red). (d) A pseudo-colored RI image of the same cell. The nucleoplasm is represented by two narrow RI ranges (blue and green) to describe the entire nucleoplasm in detail. The nucleolus (red) and cytoplasm (yellow) are represented by other RI ranges (e) A pseudo-colored RI image of the same cell, the nucleoplasm is represented by a narrow RI range (yellow) and highlighting nucleoli with three different narrow RI ranges (blue, green, red) is shown. The RI ranges used for RI rendering are depicted by pseudo-color bars (inset).

To compare biophysical properties of the nucleolus with those of other compartments, Kim et al. evaluated the RI and *D* values of the nucleolus, nucleoplasm, and cytoplasm under varying physiological conditions, such as osmotic stress, transcription inhibition, and ATP depletion. Interestingly, the study demonstrated that the biophysical properties of the nucleolus in live cells are sensitive to ATP depletion and transcriptional inhibition while insensitive to hyperosmotic pressure compared with other compartments, such as the cytoplasm and nucleoplasm, suggesting that the nucleolus has unique physicochemical properties. The unique property of the nucleolus showed by RI analysis of live cells is also in good agreement with previous studies using FCS [10,11,34]. Among them, the ODT time-lapse observation of single live cells according to ATP depletion contrasts well with previous studies using single-molecule imaging or FCS [35]. Figure 3 shows the RI analysis for three time points as a result of the time-lapse observation of a single HeLa cell immediately after ATP depletion. From the pseudo-colored RI images, the size (volume) of the nucleus (i.e., nuclear shrinkage), nucleolus, and cell decrease, and the average RI increases (Fig. 3a). Interestingly, the RI of the nucleolus increases much more than the RI of the cytoplasm with time (Fig. 3b). As shown in Figure 2e, when the RI is further subdivided and evaluated, the RI of only a specific area of the nucleolus increases [30]. Similarly, this local increase in the RI of the nucleolus could be found even under conditions that inhibit transcription using actinomycin D [30]. The decrease in *D* value in the nucleolus under ATP depletion and transcription inhibition found in previous studies using FCS is probably due to this local increase in RI [10,11].

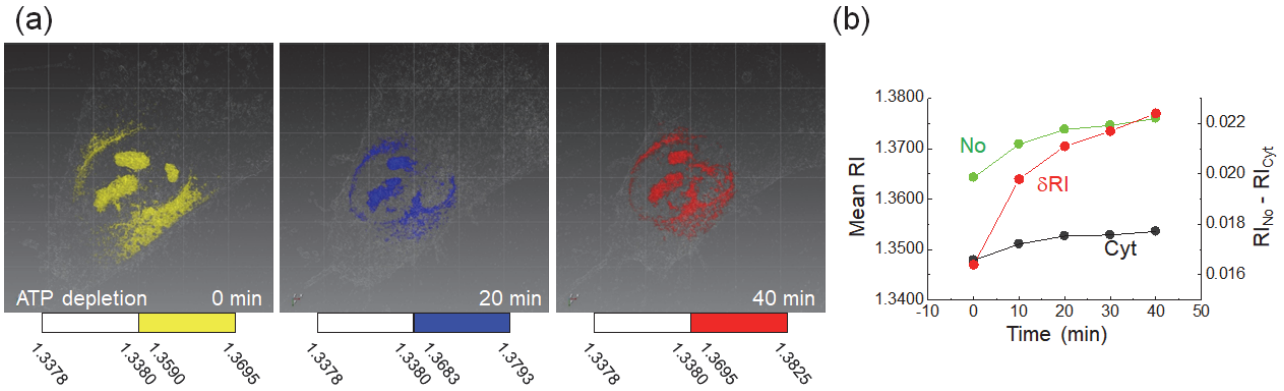

Figure 3 Optical diffraction tomography (ODT) time-lapse analysis of single HeLa cells after ATP depletion. A single HeLa cell was traced by ODT over a 40 min period following media change for ATP depletion. (a) Representative pseudo-colored refractive index (RI) images of identical HeLa cells during indicated time-lapse intervals after ATP depletion. In pseudo-colored images, the nucleolus (yellow, blue, red) and plasma membrane (white) are represented by single RI ranges, respectively. The RI ranges used for RI rendering are depicted by pseudo-color bars (inset). Note that a part of nuclear membranes and the perinuclear regions of the cytosol are also expressed in the same RI region as the nucleolus. (b) Time change of RI value of the nucleolus (No, green) and cytoplasm (Cyt, black) is shown. δRI (red) represents the difference in RI value (RI_{No}-RI_{Cyt}) between the nucleolus and the cytoplasm.

3D Imaging of Mitotic Chromosome Using ODT

Compared to human-derived HeLa cells, which have a large number of chromosomes and a small size, Indian Muntjac fibroblasts (DM cells) have a small number of chromosomes and a large size [20,36]. Therefore, when the chromosomes are fluorescently stained and observed three-dimensionally with a confocal microscope, each chromosome can be clearly distinguished [20,37]. The volume of the DM cell chromosome is sufficiently larger than the detection volume (~0.12 fL) analyzed by FCS. Therefore, the previous study utilized DM cells that simultaneously expressed H2B tagging red fluorescent protein (H2B-mRFP) and multimeric GFP of various sizes, including monomeric GFP, for quantifying the *D* value of the GFP probes by mitotic phase through CLSM imaging and FCS analysis [10,11,20,34]. As a result, the degree of freedom of movement of the nucleosome was theoretically simulated based on the *D* values. Additionally, chromosomes are known as highly dense organelles; thus, Kim et al. hypothesized that the label-free ODT method could be used to perform 3D imaging of chromosomes in various cell lines in the same way as CLSM [37]. Moreover, they predicted that a relatively detailed RI distribution would be derived with sharper chromosome images, especially when using DM cells. In the previous study, CLSM, FCS, and ODT analysis were respectively applied to DM cells simultaneously expressing H2B-mRFP and monomeric GFP to evaluate the accuracy of 3D ODT imaging and the

relationship between the RI value of the mitotic chromosome and the *D* value of the GFP probe inside the chromosome. Furthermore, Kim et al. examined the effects of osmotic stress on the RI values of mitotic cells and the *D* values of the GFP probe and demonstrated an inverse relationship between the RI and *D* in live cells during mitosis. It was also found that the chromosomes were accessible to probe molecules that diffuse freely, although hypertonic stress significantly increased the molecular density of the chromosome. Figure 4a shows time-lapsed tomographic images obtained by observing 90 minutes from prometaphase to telophase and cytokinesis after the DM cells enter the mitotic phase. For comparison, 3D images of mitotic chromosomes in different phases obtained by CLSM are also shown in Figure 4b. Since the RI values of the cell membrane, cytoplasm, and chromosome are significantly different, they can be easily expressed in pseudo-color using three different RI regions. The cell membrane and chromosome shape are clearly separated. Furthermore, compared with the 3D CLSM image of the chromosome, chromatid can be reproduced adequately with label-free ODT imaging. Although small structures with high RI values (red) and many membrane-like vesicles (green) with a medium RI are found in the cytoplasm, this is presumed to be caused by vesicles, endoplasmic reticulum, and mitochondria. Although it is also possible to analyze the RI subdivided for chromosomes, as shown in the ODT analysis of the nucleolus (Fig. 2e), it seems that additional consideration will be needed to determine which analysis is more accurate.

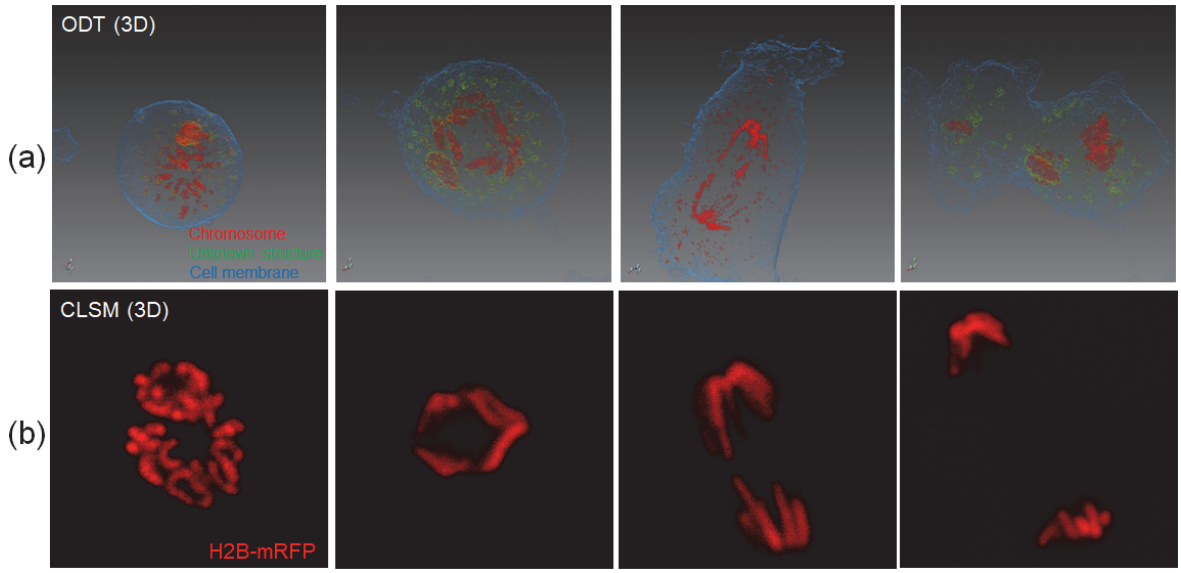

Figure 4 Comparison of 3D confocal fluorescence images of the mitotic chromosome (H2B-mRFP) with 3D refractive index (RI) images of a mitotic DM cell. (a) Four RI images of a DM cell stably expressing H2B-mRFP and mGFP from a series of time-lapse observations during mitosis (90 min). Three different RI regions of mitotic DM cells representing cell membrane (blue), chromosome (red), and unknown small vesicles (green) are shown. (b) Four fluorescence images of H2B-mRFP from a series of time-lapse and 3D observations depicting mitosis in a DM cell stably expressing H2B-mRFP and mGFP. For clarity, images from mGFP channels are not shown.

Interestingly, the average RI value of DM cell chromosomes (1.3706) was much higher than that of the nucleolus (1.3553), and HeLa cells also had a higher RI of the chromosome (1.3734) than that of the nucleolus (1.3626). The result indicates that the molecular density inside the mitotic chromosome is much higher than that of the nucleolus. On the contrary, the *D* value of the GFP probe inside the nucleolus is much smaller [10,11,30,37], demonstrating that many components or biomolecules inside the nucleolus is immobile compared to those inside the chromosome. Consequently, the studies using FCS and ODT extended the results of previous studies concerning the influence of various physiological conditions, such as osmotic stress and ATP depletion, on nuclear structure and molecular crowding effects.

Perspective

In this paper, the ODT method was introduced, which is a QPI method that has been remarkably developed in recent years. Recently, the commercialization of ODT-based holographic microscopes has made it easier to use this technology without specialized optical knowledge, and applied research is expanding in biology and medicine. Until now, label-free 3D ODT has been applied to evaluate the overall physical properties of various cells, including bacteria, red blood cells,

and culture cell lines [25-29,38-40]. Technically, the ODT method does not provide molecular specificity and has limitations in separating and analyzing spatially intermingled organelles with similar RI values, such as nuclear envelope, endoplasmic reticulum, and Golgi (Fig. 5a). Nevertheless, it provides information on the RI and volume, which are parameters of absolute quantification, directly reflecting intrinsic properties, such as the local molecular concentration of organelles. Importantly, ODT can obtain the physical properties and 3D images of various cellular organelles concurrently. In fluorescence imaging, only the distribution of labeled target molecules in cells is generally observed, and the differences under various physiological conditions are compared to the control group and evaluated. In most cases, since only a specific organelle is stained and observed, the effect of physiological changes on whole organelles cannot be obtained. In contrast, when ODT is applied, changes in volumetric and physical properties of the whole organelles can be detected, even though the accurate classification of each organelle or verification of the reliability of subdivided RI analysis is still limited. Cellular imaging that directly correlates fluorescence and ODT (Fig. 5b) will allow for a more comprehensive analysis of spatio-temporal changes both in target molecules and in surrounding organelles [41-43]. Although the correlative ODT and fluorescence method has an advantage, it should be taken into account that the use of fluorescence staining can change the original properties of cells. On the other hand, Raman spectroscopy, which is one of the other label-free microscopy methods, provides chemical information of specific elements. Therefore, if it can be combined with ODT, it will be able to overcome each other's limitations. In fact, such ODT combined Raman spectroscopy can be applied to the analysis of organelles such as lipid droplets or to discriminate cancer cells with high metastatic potential [44, 45].

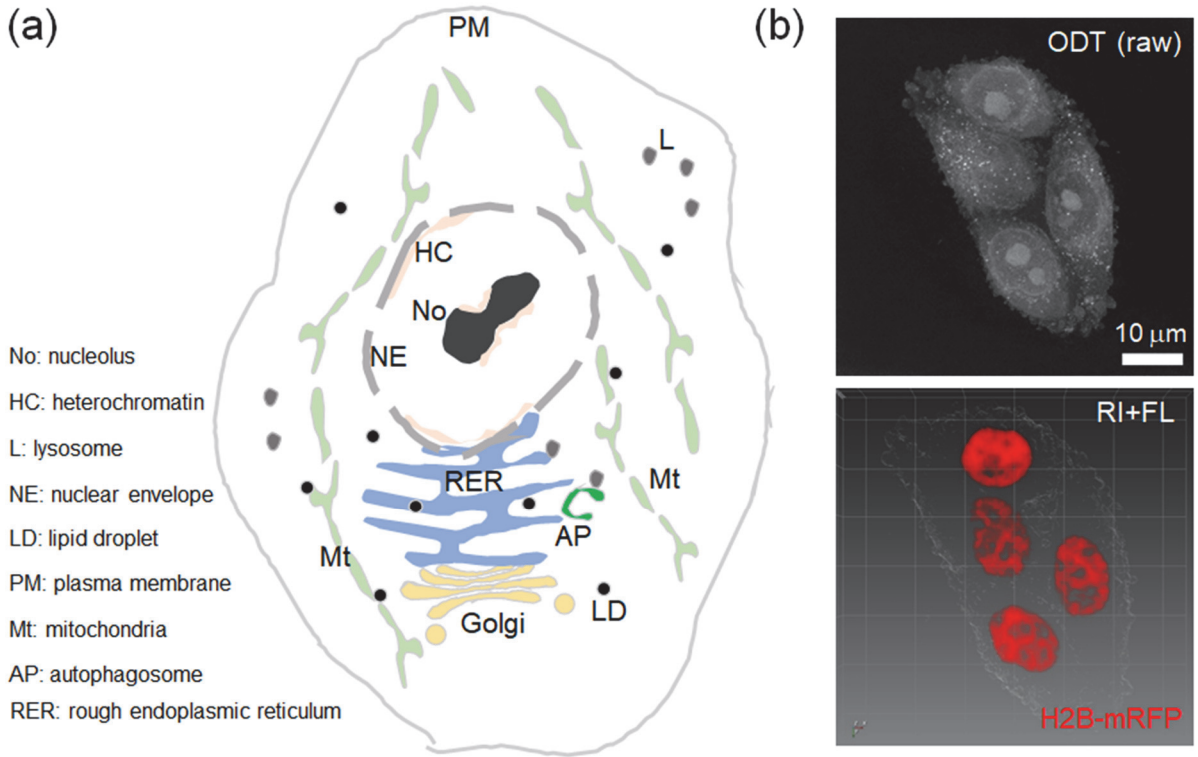

Figure 5 Correlative fluorescence and optical diffraction tomography (ODT). (a) A schematic illustration showing the various organelles of a cell. Although each organelle in cells forms a spatially complex structure, it was simplified. (b) Correlative fluorescence (red) and ODT (white, plasma membrane) image of HeLa cells expressing H2B-mRFP is shown. RI and FL stand for RI rendered and fluorescence image, respectively.

The non-invasive ODT technique is expected to have many advantages when applied to stem cell and immune cell research, which is sensitive to numerous stimuli and mainly relies on the analysis of stained fixative cells. In addition, it will be possible to quantitatively and spatially analyze the kinetic changes of organelles that respond rapidly to specific drugs or the generation and disappearance of high-density structures or aggregates [46, 47]. For example, selective autophagy that external stimuli can trigger is accompanied by the formation of large amounts of autophagosomes. However, uncovering the kinetic characteristics of these changes currently relies only on analysis using GFP/RFP tagged

system. In the future, if a confocal microscope and a QPI microscope incorporating FCS or Raman spectroscopy are developed, cell research that complementarily utilizes the advantages of each method could be conducted. ODT analysis could be an effective tool for understanding various biophysical phenomena that occur in cells.

Conflict of Interest

The author declares no conflict of interest.

Author Contributions

CGP wrote the manuscript.

Acknowledgments

I would like to thank TOMOCUBE Inc. for their technical support and discussion. I also thank Dr. Tae-Keun Kim for his technical support. This work was supported by the Basic Science Research Program (Grant No. 2018R1D1A1B07048696) through the National Research Foundation of Korea (NRF). I would like to thank Scientific Publication Team of Asan Medical Center and Editage Ltd. for English language editing.

References

[1] Elson, E. L., Magde, D. Fluorescence correlation spectroscopy. I. Conceptual basis and theory. Biopolymers 13, 1-27 (1974). https://doi.org/10.1002/bip.1974.360130102
[2] Magde, D., Elson, E. L., Webb, W. W. Fluorescence correlation spectroscopy. II. An experimental realization. Biopolymers 13, 29-61 (1974). https://doi.org/10.1002/bip.1974.360130103
[3] Aragon, S. R., Pecora, R. Fluorescence correlation spectroscopy as a probe of molecular dynamics. J. Chem. Phys. 64, 1791-1803 (1976). https://doi.org/10.1063/1.432357
[4] Rigler, R., Mets, U., Widengren, J., Kask, P. Fluorescence correlaton spectroscopy with high count rate and low background: analysis of translational diffusion. Eur. Biophys. J. 22, 169-175 (1993). https://doi.org/10.1007/BF00185777
[5] Capoulade, J., Wachsmuth, M., Hufnagel, L., Knop, M. Quantitative fluorescence imaging of protein diffusion and interaction in living cells. Nat. Biotechnol. 29, 835-839 (2011). https://doi.org/10.1038/nbt.1928
[6] Pack, C. G. Confocal laser scanning microscopy and fluorescence correlation methods for the evaluation of molecular interactions. Adv. Exp. Med. Biol. 1310, 1-30 (2021). https://doi.org/10.1007/978-981-33-6064-8_1
[7] Zernike, F. Phase contrast, a new method for the microscopic observation of transparent objects part I. Physica 9, 686–698 (1942). https://doi.org/10.1016/S0031-8914(42)80035-X
[8] Choi, W., Fang-Yen, C., Badizadegan, K., Oh, S., Lue, N., Dasari, R. R., et al. Tomographic phase microscopy. Nat. Methods 4, 717-719 (2007). https://doi.org/10.1038/nmeth1078
[9] Park, Y., Diez-Silva, M., Popescu, G., Lykotrafitis, G., Choi, W., Feld, M. S., et al. Refractive index maps and membrane dynamics of human red blood cells parasitized by *Plasmodium falciparum*. Proc. Natl. Acad. Sci. U.S.A. 105, 13730-13735 (2008). https://doi.org/10.1073/pnas.0806100105
[10] Pack, C. G., Saito, K., Tamura, M., Kinjo, M. Microenvironment and effect of energy depletion in the nucleus analyzed by mobility of multiple oligomeric EGFPs. Biophys. J. 91, 3921-3936 (2006). https://doi.org/10.1529/biophysj.105.079467
[11] Park, H., Han, S. S., Sako, Y., Pack, C. G. Dynamic and unique nucleolar microenvironment revealed by fluorescence correlation spectroscopy. FASEB J. 29, 837-848 (2015). https://doi.org/10.1096/fj.14-254110
[12] Theillet, F. X., Binolfi, A., Frembgen-Kesner, T., Hingorani, K., Sarkar, M., Kyne, C., et al. Physicochemical properties of cells and their effects on intrinsically disordered proteins (IDPs). Chem. Rev. 114, 6661-6714 (2014). https://doi.org/10.1021/cr400695p
[13] Yamaoki, Y., Nagata, T., Sakamoto, T., Katahira, M. Observation of nucleic acids inside living human cells by in-cell NMR spectroscopy. Biophys. Physicobiol. 17, 36-41 (2020). https://doi.org/10.2142/biophysico.BSJ-2020006
[14] Verkman, A. S. Solute and macromolecule diffusion in cellular aqueous compartments. Trends Biochem. Sci. 27, 27-33 (2002). https://doi.org/10.1016/S0968-0004(01)02003-5
[15] Chebotareva, N. A., Kurganov, B. I., Livanova, N. B. Biochemical effects of molecular crowding. Biochemistry (Mosc) 69, 1239-1251 (2004). https://doi.org/10.1007/s10541-005-0070-y
[16] Hancock, R. A role for macromolecular crowding effects in the assembly and function of compartments in the nucleus. J. Struct. Biol. 146, 281-290 (2004). https://doi.org/10.1016/j.jsb.2003.12.008

[17] Sasaki, Y., Miyoshi, D., Sugimoto, N. Effect of molecular crowding on DNA polymerase activity. Biotechnol. J. 1, 440-446 (2006). https://doi.org/10.1002/biot.200500032
[18] Cho, E. J., Kim, J. S. Crowding effects on the formation and maintenance of nuclear bodies: insights from molecular-dynamics simulations of simple spherical model particles. Biophys. J. 103, 424-433 (2012). https://doi.org/10.1016/j.bpj.2012.07.007
[19] Gnutt, D., Gao, M., Brylski, O., Heyden, M., Ebbinghaus, S. Excluded-volume effects in living cells. Angew. Chem. Int. Ed. Engl. 54, 2548-2551 (2015). https://doi.org/10.1002/anie.201409847
[20] Hihara, S., Pack, C. G., Kaizu, K., Tani, T., Hanafusa, T., Nozaki, T., et al. Local nucleosome dynamics facilitate chromatin accessibility in living mammalian cells. Cell Rep. 2, 1645-1656 (2012). https://doi.org/10.1016/j.celrep.2012.11.008
[21] Pack, C. G., Yukii, H., Toh-e, A., Kudo, T., Tsuchiya, H., Kaiho, A., et al. Quantitative live-cell imaging reveals spatio-temporal dynamics and cytoplasmic assembly of the 26S proteasome. Nat. Commun. 5, 3396 (2014). https://doi.org/10.1038/ncomms4396
[22] Yoon, J., Jo, Y., Kim, M. H., Kim, K., Lee, S., Kang, S. J., et al. Identification of non-activated lymphocytes using three-dimensional refractive index tomography and machine learning. Sci. Rep. 7, 6654 (2017). https://doi.org/10.1038/s41598-017-06311-y
[23] Fu, D., Choi, W., Sung, Y., Yaqoob, Z., Dasari, R. R., Feld, M. Quantitative dispersion microscopy. Biomed. Opt. Express 1, 347-353 (2010). https://doi.org/10.1364/BOE.1.000347
[24] Weast, R. C. CRC handbook of chemistry and physics (CRC Press, Boca Raton, FL, 1988).
[25] Jung, J., Kim, K., Yoon, J., Park, Y. Hyperspectral optical diffraction tomography. Opt. Express 24, 2006-2012 (2016). https://doi.org/10.1364/OE.24.002006
[26] Kemper, B., Vollmer, A., Rommel, C. E., Schnekenburger, J., von Bally, G. Simplified approach for quantitative digital holographic phase contrast imaging of living cells. J. Biomed. Opt. 16, 026014 (2011). https://doi.org/10.1117/1.3540674
[27] Kim, G., Lee, M., Youn, S., Lee, E., Kwon, D., Shin, J., et al. Measurements of three-dimensional refractive index tomography and membrane deformability of live erythrocytes from *Pelophylax nigromaculatus*. Sci. Rep. 8, 9192 (2018). https://doi.org/10.1038/s41598-018-25886-8
[28] Kim, K., Kim, K. S., Park, H., Ye, J. C., Park, Y. Real-time visualization of 3-D dynamic microscopic objects using optical diffraction tomography. Opt. Express 21, 32269-32278 (2013). https://doi.org/10.1364/OE.21.032269
[29] Kim, K., Yaqoob, Z., Lee, K., Kang, J. W., Choi, Y., Hosseini, P., et al. Diffraction optical tomography using a quantitative phase imaging unit. Opt. Lett. 39, 6935-6938 (2014). https://doi.org/10.1364/OL.39.006935
[30] Kim, T. K., Lee, B. W., Fujii, F., Kim, J. K., Pack, C. G. Physicochemical properties of nucleoli in live cells analyzed by label-free optical diffraction tomography. Cells 8, 699 (2019). https://doi.org/10.3390/cells8070699
[31] Eskiw, C. H., Dellaire, G., Mymryk, J. S., Bazett-Jones, D. P. Size, position and dynamic behavior of PML nuclear bodies following cell stress as a paradigm for supramolecular trafficking and assembly. J. Cell Sci. 116, 4455-4466 (2003). https://doi.org/10.1242/jcs.00758
[32] Morris, G. E. The Cajal body. Biochim. Biophys. Acta 1783, 2108-2115 (2008). https://doi.org/10.1016/j.bbamcr.2008.07.016
[33] Dundr, M., Misteli, T. Biogenesis of nuclear bodies. Cold Spring Harb. Perspect. Biol. 2, a000711 (2010). https://doi.org/10.1101/cshperspect.a000711
[34] Wachsmuth, M., Caudron-Herger, M., Rippe, K. Genome organization: balancing stability and plasticity. Biochim. Biophys. Acta 1783, 2061-2079 (2008). https://doi.org/10.1016/j.bbamcr.2008.07.022
[35] Shav-Tal, Y., Darzacq, X., Shenoy, S. M., Fusco, D., Janicki, S. M., Spector, D. L., et al. Dynamics of single mRNPs in nuclei of living cells. Science 304, 1797-1800 (2004). https://doi.org/10.1126/science.1099754
[36] Drpic, D., Almeida, A. C., Aguiar, P., Renda, F., Damas, J., Lewin, H. A., et al. Chromosome segregation is biased by kinetochore size. Curr. Biol. 28, 1344-1356.e5 (2018). https://doi.org/10.1016/j.cub.2018.03.023
[37] Kim, T. K., Lee, B. W., Fujii, F., Lee, K. H., Lee, S., Park, Y., et al. Mitotic chromosomes in live cells characterized using high-speed and label-free optical diffraction tomography. Cells 8, 1368 (2019). https://doi.org/10.3390/cells8111368
[38] Lee, K., Kim, K., Jung, J., Heo, J., Cho, S., Lee, S., et al. Quantitative phase imaging techniques for the study of cell pathophysiology: from principles to applications. Sensors (Basel) 13, 4170-4191 (2013). https://doi.org/10.3390/s130404170
[39] Stanly, T. A., Suman, R., Rani, G. F., O'Toole, P. J., Kaye, P. M., Hitchcock, I. S. Quantitative optical diffraction tomography imaging of mouse platelets. front. Physiol. 11, 568087 (2020). https://doi.org/10.3389/fphys.2020.568087
[40] Buzalewicz, I., Ulatowska-Jarza, A., Kaczorowska, A., Gasior-Glogowska, M., Podbielska, H., Karwanska, M., et

al. Bacteria single-cell and photosensitizer interaction revealed by quantitative phase imaging. Int. J. Mol. Sci. 22, 5068 (2021). https://doi.org/10.3390/ijms22105068

[41] Shin, S., Kim, D., Kim, K., Park, Y. Super-resolution three-dimensional fluorescence and optical diffraction tomography of live cells using structured illumination generated by a digital micromirror device. Sci. Rep. 8, 9183 (2018). https://doi.org/10.1038/s41598-018-27399-w

[42] Dong, D., Huang, X., Li, L., Mao, H., Mo, Y., Zhang, G., et al. Super-resolution fluorescence-assisted diffraction computational tomography reveals the three-dimensional landscape of the cellular organelle interactome. Light Sci. Appl. 9, 11 (2020). https://doi.org/10.1038/s41377-020-0249-4

[43] Guo, R., Barnea, I., Shaked, N. T. Limited-angle tomographic phase microscopy utilizing confocal scanning fluorescence microscopy. Biomed Opt. Express 12, 1869-1881 (2021). https://doi.org/10.1364/BOE.419598

[44] Hsieh, C.-M., Liu, P. Y., Chin, L. K., Zhang, J. B., Wang, K., Sung, K.-B., et al. Regulation of lipid droplets in live preadipocytes using optical diffraction tomography and Raman spectroscopy. Opt. Express 27, 22994-23008 (2019). https://doi.org/10.1364/OE.27.022994

[45] Paidi, S. K., Shah, V., Raj, P., Glunde, K., Pandey, R., Barman, I. Coarse Raman and optical diffraction tomographic imaging enable label-free phenotyping of isogenic breast cancer cells of varying metastatic potential. Biosens. Bioelectron. 175, 112863 (2021). https://doi.org/10.1016/j.bios.2020.112863

[46] Kim, D., Oh, N., Kim, K., Lee, S., Pack, C. G., Park, J. H., et al. Label-free high-resolution 3-D imaging of gold nanoparticles inside live cells using optical diffraction tomography. Methods 136, 160-167 (2018). https://doi.org/10.1016/j.ymeth.2017.07.008

[47] Choi, W. H., Yun, Y., Park, S., Jeon, J. H., Lee, J., Lee, J. H., et al. Aggresomal sequestration and STUB1-mediated ubiquitylation during mammalian proteaphagy of inhibited proteasomes. Proc. Natl. Acad. Sci. U.S.A. 117, 19190-19200 (2020). https://doi.org/10.1073/pnas.1920327117